

# Properties of black hole-star binaries formed in $N$ -body simulations of massive star clusters: implications for Gaia black holes

Federico Fantoccoli,<sup>1,2</sup>★ Jordan Barber,<sup>1</sup>† Fani Dosopoulou,<sup>1</sup> Debatri Chattopadhyay,<sup>1</sup> Fabio Antonini<sup>1</sup>

<sup>1</sup>Gravity Exploration Institute, School of Physics and Astronomy, Cardiff University, Cardiff CF24 3AA, UK

<sup>2</sup>Departement of Physics G. Occhialini, University of Milano Bicocca, Piazza della Scienza 3, I-20126 Milan, Italy,

Accepted XXX. Received YYY; in original form ZZZ

## ABSTRACT

We investigate black hole-star binaries formed in  $N$ -body simulations of massive, dense star clusters. We simulate 32 clusters with varying initial masses ( $10^4 M_{\odot}$  to  $10^6 M_{\odot}$ ), densities ( $1200 M_{\odot} \text{pc}^{-3}$  to  $10^5 M_{\odot} \text{pc}^{-3}$ ), and metallicities ( $Z = 0.01, 0.001, 0.0001$ ). Our results reveal that star clusters produce a diverse range of BH-star binaries, with dynamical interactions leading to extreme systems characterised by large orbital separations and high black hole masses. Of the ejected BH-main sequence (BH-MS) binaries, 20% form dynamically, while the rest originate from the primordial binary population initially present in the cluster. Ejected BH-MS binaries that are dynamically formed have more massive black holes, lower-mass stellar companions, and over half are in a hierarchical triple system. All unbound BH-giant star (BH-GS) binaries were ejected as BH-MS binaries and evolved into the BH-GS phase outside the cluster. Due to their lower-mass companions, most dynamically formed binaries do not evolve into BH-GS systems within a Hubble time. Consequently, only 2 of the 35 ejected BH-GS binaries are dynamically formed. We explore the formation pathways of Gaia-like systems, identifying two Gaia BH1-like binaries that formed through dynamical interactions, and two Gaia BH2-like systems with a primordial origin. We did not find any system resembling Gaia BH3, which may however be attributed to the limited sample size of our simulations.

**Key words:** stars: kinematics and dynamics, methods: numerical, stars: black holes, globular clusters: general, galaxies: star clusters: general

## 1 INTRODUCTION

Black hole binaries, particularly black hole-star (BH-S) systems, have long been essential for studying the formation and evolution of massive stars (e.g., Eggleton 2006; McClintock & Remillard 2006). Historically, most of our understanding of black holes (BHs) comes from the study of X-ray binaries, where the BH mass could be dynamically measured (e.g., Özel et al. (2010); Farr et al. (2011)). These systems represent an important observational benchmark for theoretical models of BH formation. In 2015, the LIGO–Virgo collaboration detected the merger of two BHs, marking the start of a new era in BH research (Abbott et al. 2016). This breakthrough has since led to the detection of more than 100 gravitational-wave (GW) events from BH and neutron star (NS) mergers (Abbott et al. 2021a,b), greatly expanding our understanding of BH populations.

In addition to gravitational wave (GW) discoveries, recent observations have revealed a new family of quiescent, or X-ray silent, BHs in binary systems. These quiescent BHs, discovered through astrometry and radial velocity measurements (e.g., Thompson et al. 2019; Liu et al. 2019), have opened new windows into the study of non-interacting BH binaries. The Gaia satellite, in particular, has been instrumental in identifying these systems. Recent Gaia discov-

eries include three quiescent BH binaries: Gaia BH1 (El-Badry et al. 2023a; Chakrabarti et al. 2023), Gaia BH2 (El-Badry et al. 2023b; Tanikawa et al. 2023b), and Gaia BH3 (Gaia Collaboration et al. 2024). These systems, with their unique orbital characteristics and associations with distinct Galactic populations, challenge traditional models of BH formation, particularly those involving isolated stellar binary evolution.

The observed properties of Gaia BHs are reported in Table 1. Gaia BH1 is a binary with a Sun-like star orbiting a BH with a mass  $\sim 10 M_{\odot}$ , an eccentricity  $e \approx 0.45$ , and a period of 186 days. Gaia BH2 is a binary with a red giant orbiting a  $9 M_{\odot}$  BH, with an eccentricity  $e \approx 0.5$ , and a relatively long period of 1280 days. Studies have investigated the formation of Gaia BH1 and Gaia BH2 through isolated mechanisms (Kotko et al. 2024; Kruckow et al. 2024; Gilkis & Mazeh 2024), however their peculiar orbital properties, such as long orbital periods and high eccentricity might be a challenge for these binary evolution models. For this reason, several previous studies using  $N$ -body simulations have investigated the possibility that these types of systems were dynamically formed in open star clusters (Shikauchi et al. 2020; Rastello et al. 2023; Di Carlo et al. 2024; Tanikawa et al. 2023a).

Gaia BH3 is composed of a  $33 M_{\odot}$  BH with a metal-poor giant star of mass  $0.76 M_{\odot}$  and metallicity  $[\text{Fe}/\text{H}] \approx -2.6$ . The binary has an eccentricity of  $e \approx 0.73$ , and a long period  $\approx 4250$  days. It has been shown that Gaia BH3 can be either explained as an outcome of

★ f.fantoccoli@campus.unimib.it

† barberj2@cardiff.ac.uk

the evolution of an isolated binary with low metallicity (Iorio et al. 2024; El-Badry 2024), or that it might have formed in a globular cluster through dynamical interactions (Marín Pina et al. 2024). Its low metallicity and chemical composition further suggest it may be part of the ED-2 stream, a remnant of a dissolved globular cluster (Balbinot, E. et al. 2024). These discoveries highlight the significance of understanding the formation pathways of black hole-star (BH-S) systems, particularly in diverse environments such as the Galactic plane, stellar halo, and dense star clusters. They also emphasise the need for more comprehensive models that incorporate both stellar evolution and dynamical processes in the formation of black hole binaries.

In this work we use detailed  $N$ -body simulations of dense and massive star clusters to characterise the properties of the BH-S binaries formed in these models. By using the highly efficient  $N$ -body code PeTar developed by Wang et al. (2020b), we extend the explored parameter space to clusters with higher masses and densities than previous work (Rastello et al. 2023; Di Carlo et al. 2024; Tanikawa et al. 2023a), including stellar evolution and a realistic initial population of massive binary stars. We investigate whether dynamical interactions in these models can generate binaries with properties resembling those of the observed Gaia black holes, and we explore potential constraints on a cluster-origin hypothesis for these systems.

The paper is organised as follows: in Section 2 we describe the simulations and their initial conditions, in Sections 3, 4, 5 and 6 we describe the properties of the ejected sample of BH-main sequence (MS), BH-giant star (GS), BH-white dwarf (WD) and NS-S (NS-MS, NS-GS) binaries produced in our simulations. In addition, we give a qualitative description of the influence of common envelope (CE), tidal interactions and triple dynamics on the orbital properties of these systems.

In Section 7, we describe the formation of Gaia BH-like systems. In Section 8 we study the formation efficiency of BH-MS and BH-GS systems in our simulations and compare our results with previous literature.

## 2 METHODS

In this work we use the high-performance hybrid  $N$ -body code PeTar (Wang et al. 2020b) to simulate 32 stellar clusters with initial cluster masses ( $M_c$ ) ranging from  $10^4 M_\odot$  to  $10^6 M_\odot$ , initial half-mass densities ( $\rho_h$ ) from  $1200 M_\odot \text{pc}^{-3}$  to  $10^5 M_\odot \text{pc}^{-3}$  and metallicities  $Z \in \{10^{-2}, 10^{-3}, 10^{-4}\}$ . PeTar makes use of the  $PT + PP$  method introduced in Oshino et al. (2011), which combines a direct  $N$ -body (particle-particle) method with a Barnes-Hut tree (particle-tree) method (Barnes & Hut 1986). Few body interactions are computed using a combination of the fourth-order Hermite integrator and the slow-down time-transformed symplectic integrator (SDAR Wang et al. 2020a). In addition, PeTar exploits parallelisation via a hybrid parallel method based on the FDPS framework (Iwasawa et al. 2016, 2020; Namekata et al. 2018). The simulation code is configured to make use of OpenMP and MPI processes for parallelisation and performs long-range force calculations with Nvidia P100 GPUs, all of which reduce the computational cost compared to other  $N$ -body codes. The lower computational cost enables us to more extensively explore the initial cluster parameter space, specifically allowing for the modelling of massive and dense clusters over multiple relaxation timescales.

Stellar and binary evolution is included in our models and is computed using the binary stellar evolution packages SSE and BSE (Hurley et al. 2000, 2002; Banerjee et al. 2020). While PeTar does not directly

compute any post-Newtonian (PN) terms within the equations of motion, compact objects can coalesce through GW emission following the semi-major axis and eccentricity evolution as described in Peters (1964).

### 2.1 Initial conditions

We initialise our cluster conditions using McLuster (Wang et al. 2019; Küpper et al. 2011), adopting a King density profile (King 1966) with a concentration parameter  $W_0 = 8$ . We do not include the effect of a galactic tidal field in any of our simulations. Most models have an initial half-mass density  $\rho_h = 1.2 \times 10^3 M_\odot \text{pc}^{-3}$  as this is a typical value found for globular clusters in the Galaxy (Harris et al. 2013). We also explore higher densities,  $\rho_h = 10^4 M_\odot \text{pc}^{-3}$  and  $\rho_h = 10^5 M_\odot \text{pc}^{-3}$ , and vary the initial cluster mass from  $10^4 M_\odot$  to  $10^6 M_\odot$ . We consider three values of metallicity:  $Z = 0.01, 0.001$  and  $0.0001$ .

For most cluster models we consider two variations. In one there are no binaries at the initialisation of the cluster and for the other variation we ensure every star with mass  $\geq 20 M_\odot$  is initialised in a binary. The latter choice is motivated by observations of young clusters and associations in which there is a large binary fraction ( $> 70\%$ ) amongst these massive stars (Sana et al. 2012). Binaries formed with the formation of the cluster are commonly termed *primordial* binaries. We note that since our primordial binaries are always set such that the primary mass is  $\geq 20 M_\odot$ , we are not considering the formation of BH-S binaries through exchanges that involve a primordial binary in which both components are low-mass stars. This is unlikely to affect significantly our results since such binaries are unlikely to undergo frequent dynamical interactions leading to an exchange of one of the components with a massive star or a BH. Due to their lower mass these binaries do not efficiently migrate to the cluster core where these interactions can take place (Spitzer 1987). However, we note that we might be underestimating the number of BH-S binaries formed.

To initialise the stellar masses of the cluster particles we adopt a Kroupa (2001) initial mass function with  $0.08 M_\odot \leq M \leq 150 M_\odot$ . Primordial binaries are then generated by taking every star with mass  $\geq 20 M_\odot$  and finding an ideal companion mass by drawing from a uniform mass ratio ( $q$ ) distribution with  $0.1 \leq q \leq 1$ ; the particle in the cluster with the closest mass to what was drawn is then chosen as the binary partner. The adopted uniform mass ratio distribution is consistent with what derived observationally (Moe & Di Stefano 2017). The eccentricity for these binaries is then drawn from a Sana et al. (2012) distribution

$$f_e = 0.55e^{-0.45}. \quad (1)$$

The binary period is set using the extended Sana et al. (2012) distribution described in Oh et al. (2015)

$$f_{\log_{10}(P)} = 0.23 \left[ \log_{10} \left( \frac{P}{\text{days}} \right) \right]^{-0.55}. \quad (2)$$

We draw supernova (SN) natal kicks from a Maxwellian distribution with  $\sigma = 265 \text{ km s}^{-1}$  (Hobbs et al. 2005) and assume a fallback kick prescription when scaling the kicks for BH formation (Fryer 1999). In addition, we assume a Fryer et al. (2012) rapid SN engine for the compact object remnant mass, and strong pulsational pair instability (PPI) cut-off at  $45 M_\odot$  (Belczynski et al. 2020). Unlike previous studies (Rastello et al. 2023; Di Carlo et al. 2024; El-Badry et al. 2022), we allowed the binary to survive without merging if a phase of common-envelope evolution is initiated by a donor star that is on the Hertzsprung gap.

|          | Stellar type         | $M_{\text{BH}} [M_{\odot}]$ | $M_* [M_{\odot}]$      | $a [R_{\odot}]$               | $P [\text{days}]$        | $e$                          | [Fe/H] |
|----------|----------------------|-----------------------------|------------------------|-------------------------------|--------------------------|------------------------------|--------|
| Gaia BH1 | G-type main-sequence | $9.62^{+0.18}_{-0.18}$      | $0.93^{+0.05}_{-0.05}$ | $301.55^{+2.15}_{-2.15}$      | $185.59^{+0.05}_{-0.05}$ | $0.45^{+0.005}_{-0.005}$     | -0.2   |
| Gaia BH2 | Red giant            | $8.94^{+0.34}_{-0.34}$      | $1.07^{+0.19}_{-0.19}$ | $1066.55^{+17.20}_{-17.20}$   | $1276.7^{+0.6}_{-0.6}$   | $0.5176^{+0.0009}_{-0.0009}$ | -0.2   |
| Gaia BH3 | G-type giant         | $32.7^{+0.82}_{-0.82}$      | $0.76^{+0.05}_{-0.05}$ | $2477.035^{+58.058}_{58.058}$ | $4253.1^{+98.5}_{-98.5}$ | $0.7291^{+0.0048}_{-0.0048}$ | -2.6   |

**Table 1.** Main properties of Gaia BH1 (El-Badry et al. 2023a), Gaia BH2 (El-Badry et al. 2023b), and Gaia BH3 (El-Badry 2024).

The largest integration time simulated was 3 Gyr with the majority of simulations integrated for 1 Gyr. The final integration time of the simulations is chosen such that it is several times the initial relaxation time of the cluster. For the most massive clusters ( $M_c = 5 \times 10^5 M_{\odot}$  and  $10^6 M_{\odot}$ ), we make sure that the simulation runs for at least half the initial relaxation time.

The first five columns of Table 2 are adapted from Barber & Antonini (2024) and provide a breakdown of the cluster initial conditions for each of our simulations.

## 2.2 Classification and post-ejection evolution

In this section, we present the two classification criteria for the binaries. Firstly, we classify the binaries as *ejected* binaries and *retained* binaries. In this paper we will mostly focus on the ejected population, which are binaries that are ejected from the cluster either by a SN kick or through a dynamical interaction. We focus on the ejected binaries since they are more relevant to the halo/field population observed by Gaia. However, we also provide a less detailed description of the retained binaries. There are two conditions that must be fulfilled to classify a binary as ejected from the cluster: firstly, we impose  $r_{\text{bin}} > 20r_{\text{h}}$ , where  $r_{\text{bin}}$  is the position of the centre of mass of the binary and  $r_{\text{h}}$  is the cluster half-mass radius at any given time. The second criterion is that the velocity of the centre of mass of the binary is larger than the escape velocity from the cluster. If these conditions are both satisfied at a given evolutionary stage (e.g., BH-MS), then the binary is classified as ejected. For the remaining binaries we only include them in our retained binary population after imposing a condition that the binary survives inside the cluster until at least the next stage of stellar evolution, e.g., a MS star becoming a GS. Thus, a retained binary is a binary that is formed as a BH-type binary inside the cluster, and it evolves to another type within the cluster.

The second classification is to divide the ejected binaries in primordial and dynamical. Primordial are the binaries initially present in the cluster, though they may experience dynamical processes that change their orbit. Dynamical binaries are those in which the components are paired through gravitational encounters during the simulations. We take the binaries at the time of ejection and subsequently evolve them in isolation for a Hubble time, using the COSMIC code (Breivik et al. 2020). All the stellar evolution parameters in COSMIC are set to be exactly the same as in PeTar so that the stellar evolution is consistent through the evolution. However, we note that the isolated evolution of an ejected binary might not be a good approximation in some cases. If the binary is ejected in a stable multiple system (triple, quadruple or more), the isolated binary evolution set-up will ignore the effect of the tertiary (or other objects in a multiple system) on the binary evolution (Stegmann et al. 2022).

The total number of primordial and dynamical binaries for each of our simulations is provided Table 2, each split into the ejected and retained populations and then further split into the stellar type of the binary components. We consider binaries in which one component is a BH and the other component is either a MS star, a WD, or a GS. We also briefly consider binaries in which one component is a NS

and the other is a star (either a MS or a GS). We discuss in detail the properties of these systems in the following sections.

## 3 BH-MS BINARIES

In this section, we characterise the ejected BH-MS population; MS stars are defined following the BSE classification of stellar types in Hurley et al. (2002). The component mass and orbital properties of the ejected BH-MS binaries are shown in Fig. 1. We consider two evolutionary times when performing the analysis: (i) the first time the stellar component is on the MS, and (ii) the last time-step in which the stellar component is classified as a MS. The aim is to illustrate the range of parameter space that a system can explore throughout its lifetime as a BH-MS binary, considering that stellar evolution processes, tidal interactions, and mass transfer events may still influence the properties of the binary. The contours represent the ‘region of similarity’ in the parameter space for the Gaia BH1 system. They are defined by the following limits:  $M_* \in [0.5, 1.5] M_{\odot}$ ,  $M_{\text{BH}} \in [8, 12] M_{\odot}$ ,  $e \in [0.2, 0.7]$ ,  $a \in [200, 600] R_{\odot}$ ,  $P \in [80, 500]$  days. These contours are much wider than the errors on the Gaia BH1-system parameters (reported in Table 1), typically smaller than 2%, and highlight the *Gaia BH1-like binaries* – for a similar analysis in lower mass cluster simulations see Rastello et al. (2023).

The distributions of the BH and MS star masses for dynamical and primordial binaries show that the two populations are well separated. For primordial binaries, the BH mass distribution is peaked around  $M_{\text{BH}} \approx 7 M_{\odot}$ , while for dynamically formed binaries the distribution is nearly uniform between  $10 M_{\odot}$  and  $40 M_{\odot}$ . This discrepancy underlines the possibility for dynamically formed binaries to cover a wider range of mass ratios compared to primordial binaries. The MS mass distribution for dynamical and primordial binaries is also distinctly separated. The primordial binary distribution has a strong peak around  $M_* \approx 30 M_{\odot}$ , while the dynamical population produces essentially no binaries near this peak, extending to both lower and higher masses and containing a large fraction of lower mass stars with a peak at around  $M_* \approx 0.45 M_{\odot}$ . We find that 93% of the ejected BH-MS binaries are formed inside the cluster. The eccentricity and period distributions for primordial and dynamical binaries cover a similar range of values, with no differing features. Moreover, we do not find significant difference in the distributions between the initial and final time of the MS evolutionary stage.

Fig. 1 shows that the eccentricity distribution has a peak at  $e \approx 0$ , and above  $e \approx 0$  the distribution appears nearly uniform. The peak could be due to a CE phase; 18% of BH-MS ejected system progenitors undergo a CE phase before ejection. As a caveat we note that post common envelope systems might have eccentricities up to  $\sim 0.2$  and that the evolution in this phase remains uncertain (Kruckow et al. 2021). In addition to a CE phase, tidal forces in the binary contribute to the circularisation of the orbit (Hurley et al. 2002; Hut 1981). The strength of both equilibrium and dynamical tides depends on the ratio between the radius of the star and the semi-major axis of the orbit ( $R/a$ ), and the binary mass ratio. Given these scales, we

| Model       | Metallicity | Total Mass<br>$M_{\odot}$ | Density<br>$M_{\odot} \text{pc}^{-3}$ | Binary Fraction | Primordial<br>BH-MS(BH-GS)[BH-WD]NS-S |               |                | Dynamical<br>BH-MS(BH-GS)[BH-WD]NS-S |            |            |          |
|-------------|-------------|---------------------------|---------------------------------------|-----------------|---------------------------------------|---------------|----------------|--------------------------------------|------------|------------|----------|
|             |             |                           |                                       |                 | Ejected                               | Retained      | Total          | Ejected                              | Retained   | Total      |          |
| Z1-M1-D3    | 0.01        | 10,000                    | 1200                                  | 0               | 0(0)[0]0                              | 0(0)[0]0      | 0(0)[0]0       | 0(0)[0]0                             | 0(0)[0]0   | 0(0)[0]0   |          |
| Z1-M5-D3    |             | 50,000                    | 1200                                  | 0.0025          | 1(1)[0]0                              | 2(2)[0]0      | 3(3)[0]0       | 0(0)[0]0                             | 1(1)[0]0   | 1(1)[0]0   |          |
| Z1-M10-D3   |             | 100,000                   | 1200                                  | 0               | 0(0)[0]0                              | 0(0)[0]0      | 0(0)[0]0       | 1(0)[0]0                             | 0(0)[0]0   | 1(0)[0]0   |          |
| Z1-M50-D3   |             | 500,000                   | 1200                                  | 0.0026          | 3(2)[1]4                              | 7(3)[0]2      | 10(5)[1]6      | 0(0)[0]0                             | 0(1)[0]0   | 0(1)[0]0   |          |
| Z1-M100-D3  |             | 1,000,000                 | 1200                                  | 0               | 0(0)[0]0                              | 0(0)[0]0      | 0(0)[0]0       | 0(0)[0]0                             | 0(0)[0]0   | 0(0)[0]0   |          |
| Z2-M1-D3    | 0.001       | 10,000                    | 1200                                  | 0               | 0(0)[0]0                              | 0(0)[0]0      | 0(0)[0]0       | 0(0)[0]0                             | 0(2)[0]0   | 0(2)[0]0   |          |
| Z2-M5-D3    |             | 50,000                    | 1200                                  | 0               | 2(1)[0]1                              | 3(3)[0]0      | 5(4)[0]1       | 0(0)[1]0                             | 1(0)[0]0   | 1(0)[1]0   |          |
| Z2-M5-D3-L  |             | 50,000                    | 1200                                  | 0.0025          | 0(0)[0]0                              | 0(0)[0]0      | 0(0)[0]0       | 0(0)[0]0                             | 0(0)[0]0   | 0(0)[0]0   |          |
| Z2-M10-D3   |             | 100,000                   | 1200                                  | 0               | 2(0)[1]0                              | 17(25)[0]0    | 19(25)[1]0     | 0(0)[0]0                             | 0(0)[0]0   | 0(0)[0]0   |          |
| Z2-M10-D3-L |             | 100,000                   | 1200                                  | 0.0026          | 0(0)[0]0                              | 0(0)[0]0      | 0(0)[0]0       | 0(0)[0]0                             | 0(0)[0]0   | 0(0)[0]0   |          |
| Z2-M10-D4   |             | 100,000                   | 10,000                                | 0               | 0(0)[2]0                              | 21(24)[0]1    | 21(24)[2]1     | 0(0)[0]0                             | 0(2)[0]0   | 0(2)[0]0   |          |
| Z2-M1-D5    |             | 10,000                    | 100,000                               | 0               | 0(0)[0]0                              | 0(0)[0]0      | 0(0)[0]0       | 0(0)[0]0                             | 0(1)[0]0   | 1(0)[0]0   |          |
| Z2-M5-D5    |             | 50,000                    | 100,000                               | 0.0025          | 9(4)[1]9                              | 47(49)[0]2    | 56(53)[1]11    | 0(0)[0]0                             | 3(2)[0]0   | 3(2)[0]0   |          |
| Z3-M1-D3    |             | 0.0001                    | 10,000                                | 1200            | 0                                     | 0(0)[0]0      | 0(0)[0]0       | 0(0)[0]0                             | 0(0)[0]0   | 0(0)[0]0   | 0(0)[0]0 |
| Z3-M5-D3    |             |                           | 50,000                                | 1200            | 0                                     | 0(0)[0]0      | 0(0)[0]0       | 0(0)[0]0                             | 0(0)[0]0   | 1(2)[0]0   | 1(2)[0]0 |
| Z3-M10-D3   | 100,000     |                           | 1200                                  | 0.0025          | 4(2)[1]3                              | 34(34)[0]2    | 38(36)[1]5     | 0(0)[0]0                             | 1(5)[0]0   | 1(5)[0]0   |          |
| Z3-M50-D3   | 500,000     |                           | 1200                                  | 0               | 0(0)[0]0                              | 0(0)[0]0      | 0(0)[0]0       | 0(0)[0]0                             | 0(0)[0]0   | 0(0)[0]0   |          |
| Z3-M100-D3  | 1,000,000   |                           | 1200                                  | 0               | 0(0)[0]0                              | 0(0)[0]0      | 0(0)[0]0       | 0(0)[0]0                             | 0(0)[0]0   | 0(0)[0]0   |          |
| Total       |             | 4,580,000                 |                                       |                 | 66(33)[17]40                          | 311(338)[0]17 | 377(371)[17]57 | 19(2)[4]0                            | 21(30)[1]0 | 40(32)[5]0 |          |

**Table 2.** Initial cluster conditions for our PeTar  $N$ -body simulations. Each model is given a unique name based on its initial setup (metallicity, initial cluster mass and density). Models with a -L added are run for 3 Gyr; Z1-M100-D3 and Z3-M50-D3 are terminated at 507 Myr, and Z3-M100-D1 and Z3-M100-D3 at 254 Myr. All the remaining models are evolved up to a maximum integration time of 1 Gyr. Each model contains two variations, one which starts with no binaries, and one which sets an initial binary fraction of 100% amongst massive stars (initial mass  $\geq 20 M_{\odot}$ ).

can approximately track the impact of tides by searching for Roche lobe overflow (RLO) events in the binary sample. During a RLO phase, the radius of one of the two stars (or both) strongly increases, enhancing the effects of tides and leading to orbital circularisation. We find that 68% of the ejected BH-MS binaries progenitors undergo at least one RLO phase before ejection. It is important to underline that all the BH-MS progenitors that undergo a CE phase, previously start a RLO overflow event. Therefore, the orbit of 26% of the systems that undergo a RLO is immediately circularised due to a CE phase. These binaries are the low eccentricity population shown in Fig. 1.

We note, however, that Sepinsky et al. (2007); Dosopoulou & Kalogera (2016a,b), showed that tidal interactions do not always result in rapid circularisation during the early stages of mass transfer. As a result, mass transfer at periastron in eccentric orbits may introduce significant eccentricities.

In addition, we underline that CE evolution and tides are not the only processes that affect the eccentricity distribution: the eccentricity distribution still remains nearly uniform due to kicks during BH formation (though attenuated in our prescription) or due to dynamical interactions in the cluster. Moreover, a more detailed analysis of the effect of tides and mass transfer is needed to fully address their role in our models, but this is beyond the scope of this work.

After ejection, no BH-MS binary experiences a CE phase (the CE phase generally occurs as the star is leaving the MS). However, 32% of the ejected BH-MS undergo at least one RLO event; this shifts

more binaries towards lower eccentricities in the final population, explaining the stronger peak at  $e \sim 0$  in the orange distribution in Fig. 1.

As previously mentioned, the presence of a tertiary companion can alter the evolution of the inner BH-MS binary (or its progenitors), leading to a different evolutionary path. In addition, Tanikawa et al. (2023a) has shown that Gaia BH-like binaries are often found with an accompanying tertiary star. Therefore we look for triple companions to the BH-MS binaries before the time of ejection. We find that 42% of the binaries have been in a stable triple system before they are ejected from the cluster. We define a *stable* triple as a system that has an outer eccentricity  $e < 1$ . We find that 37% of the stable triples occur when the inner binary is a BH-MS. Moreover, in the majority of these systems (85%), the inner binary is dynamically formed. When analysing the properties of the triples in our models, we look at the last evolution snapshot in which the system is present in the simulation: they have an average semi-major axis ratio  $a_{\text{in}}/a_{\text{out}} = 0.015$  (where  $a_{\text{in}}$  is the semi-major axis of the inner orbit and  $a_{\text{out}}$  of the outer orbit), and the average outer orbital eccentricity is  $e = 0.93$ .

Out of the 85 ejected BH-MS binaries, only 13 are found in stable triple systems. This implies that in at least 85% of cases, treating the binary as isolated is a reasonable approximation for its evolution after ejection from the cluster. We find that in 11 of the 13 ejected triple systems the inner binary is from the dynamical population. Thus, 68% of the ejected dynamical BH-MS binaries, and 3% of the



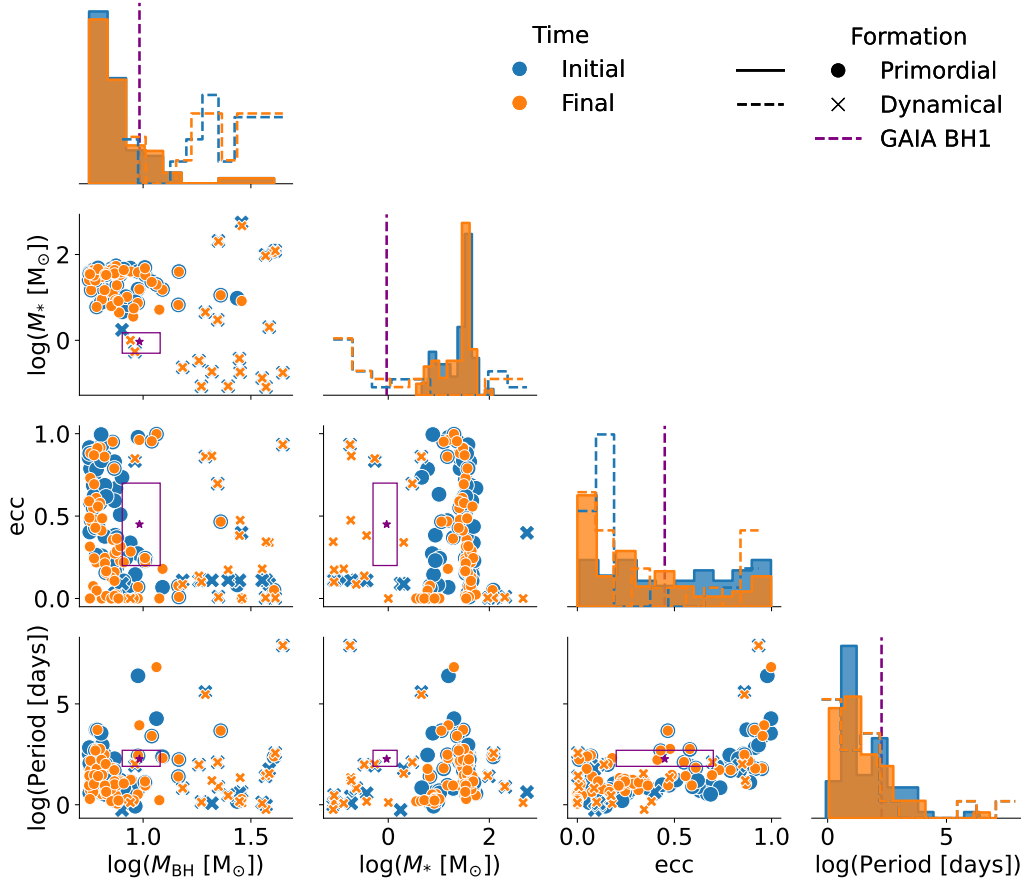


**Figure 1.** Component mass and orbital properties of the ejected BH-MS binaries. In the scatter(histogram) plots, dots(lines) and crosses(dashes) represent primordial binaries and dynamical binaries, respectively; binaries at the first BH-MS time are in blue and at the last BH-MS time in orange. The purple contours define the Gaia BH1 similarity region.

ejected primordial BH-MS binaries are in a stable triple at ejection. This suggests that the presence of a tertiary companion is a signature of dynamical formation in our models.

### 3.1 BH-MS retained binaries

We consider now the properties of the retained BH-MS binaries in our simulations, the properties of which are shown in Fig. 2. We note that we found no substantial change between the main properties of BH-MS binaries at the time of formation and at the last BH-MS time. Therefore, we show only the binaries taken at the final BH-MS time. However, we do keep the distinction between primordial and dynamical binaries and find that 94% of the binaries have a primordial origin, while 6% are formed dynamically.

The distributions shown in Fig. 2 are similar to those in Fig. 1. The BH mass distribution shows an evident cut-off at  $\approx 45 M_{\odot}$ . This sharp mass limit is due to PPI SN that prevents the formation of any BHs above this mass value. The few binaries that cross the threshold have a dynamical origin, and are either formed through hierarchical binary black hole (BBH) mergers or through the accretion of a massive star by a BH (Barber & Antonini 2024). It is important to point out that currently PeTar does not compute a GW recoil kick following a BBH merger. Therefore, some of the massive BHs formed through hierarchical mergers that we find, will likely be ejected from the cluster shortly after forming and thus not go on to form future binaries.

We note that the population of dynamically formed binaries contains a significant sub-population with  $M_* \lesssim 1 M_{\odot}$  – the median MS mass of this clump is  $\approx 0.44 M_{\odot}$ . These binaries are formed early during the simulation and, in almost all cases, are immediately disrupted: the median formation time is  $\approx 4.11$  Myr from the beginning of the simulation, and the median disruption time is the same. Therefore most of them undergo an immediate disruption after formation and are not shown in Fig. 2.

On the other hand, for ejected BH-MS binaries, the population of the corresponding low mass clump is made of 13 binaries: 3 binaries survive as BH-MS for an average time  $\approx 971$  Myr, the other 10 stay BH-MS until the end of the simulation. The most similar binary to Gaia BH1 (see Section 7.1) is part of this long-lived population.

## 4 BH-GS BINARIES

In this section, we describe the BH-GS binary population in our models; GSs are defined following the BSE classification as stars with indices 3, 4, or 5 (e.g., Di Carlo et al. 2024). The results are reported in Fig. 3. The Gaia BH2 similarity region is defined as:  $M_* \in [0.5, 1.2] M_{\odot}$ ,  $M_{BH} \in [8, 12] M_{\odot}$ ,  $e \in [0.2, 0.7]$ ,  $a \in [238, 1088] R_{\odot}$ ,  $P \in [200, 2000]$  days, while for Gaia BH3  $M_* \in [0.2, 1] M_{\odot}$ ,  $M_{BH} \in [25, 45] M_{\odot}$ ,  $e \in [0.5, 0.9]$ ,  $a \in [560, 11760] R_{\odot}$ ,  $P \in [400, 40000]$  days; the same contours for Gaia BH3 are adopted in Marín Pina et al. (2024). All the ejected

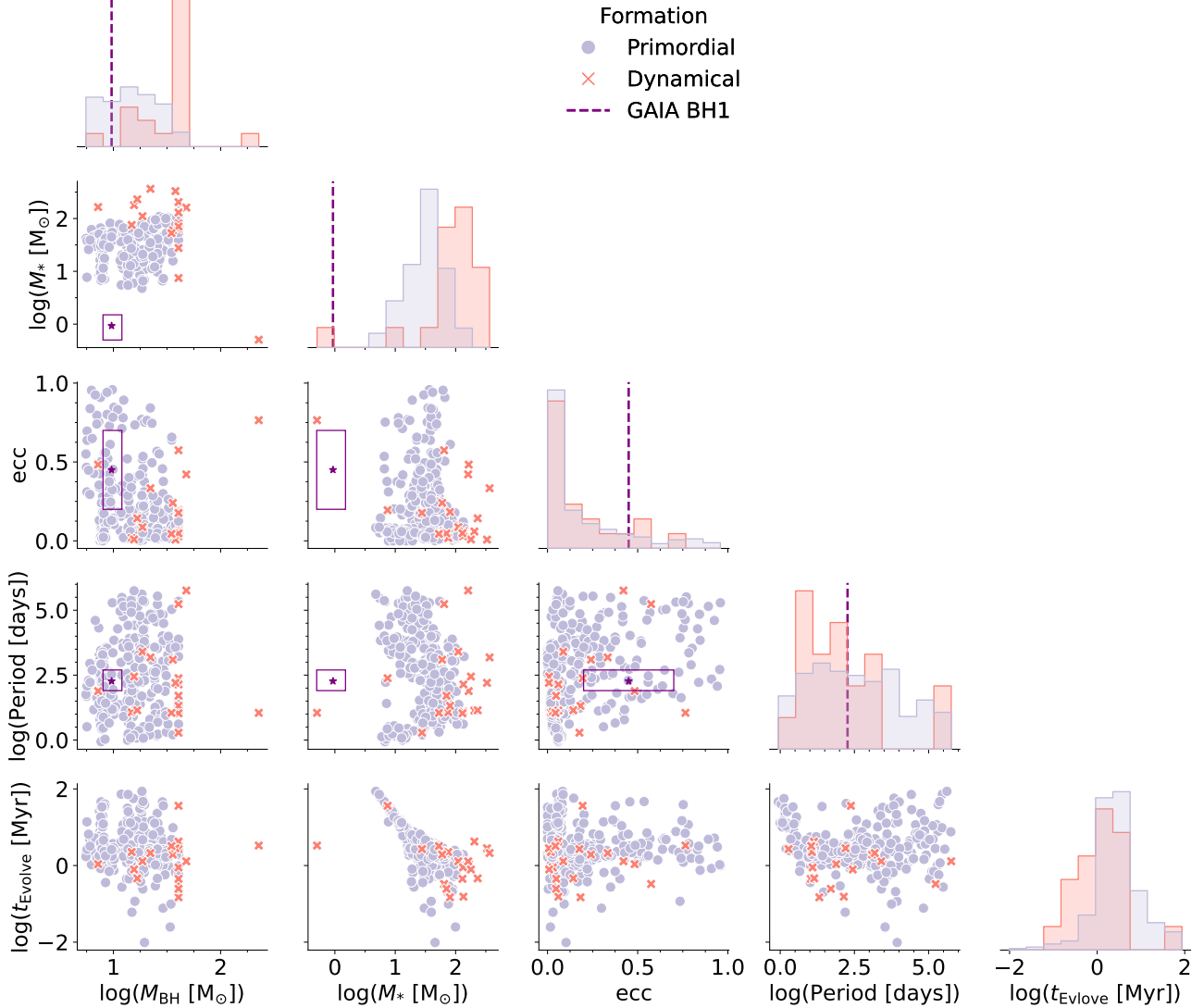


**Figure 2.** Properties of BH-MS retained binaries. Red dots and the blue crosses represent primordial binaries and dynamical binaries, respectively; the purple contours depict the Gaia BH1 similarity region. Here  $t_{\text{evolve}}$  represents the lifetime of the binary, i.e., the time between formation and when the stellar component evolves off the MS.

BH-GS binaries in our models are first ejected as BH-MS binaries and then evolve to a BH-GS binary outside the cluster.

From Fig. 3 it is evident that almost all the BH-GS ejected systems are from the primordial binary population with the BH mass peak at  $M_{\text{BH}} \approx 8 M_{\odot}$ , similarly to the BH-MS case; the eccentricity distribution has a strong peak near  $e \approx 0$ . The only systems that have  $e > 0$  have a GS mass in the range  $M_* \in [10, 35] M_{\odot}$ . Roughly half of these systems maintain a finite eccentricity up to the end of the BH-GS phase, in the other half the eccentricity drops to  $e = 0$ . As previously discussed for BH-MS binaries, the evolution towards  $e \approx 0$  is driven by tides and CE evolution. We find 63% of BH-GS progenitors undergo a RLO event that reduces the median of the eccentricities from  $\approx 0.21$  pre-RLO to  $\approx 0$  post-RLO, and 37% of the systems undergo a CE phase.

After ejection, 26% of BH-GS undergo a CE phase when they are classified as BH-GS and 49% experience a RLO phase. Moreover, in the vast majority of cases, the RLO phase occurs when the stellar companion is a Hertzsprung gap (HG) star. Unlike the BH-MS

case, the number of dynamically formed systems (2) is significantly lower compared to the primordial binaries (33), making it difficult to provide a meaningful comparison between the two populations.

As for the BH-MS binaries, we look for triple systems in our BH-GS sample. We consider the 35 ejected BH-GS binaries that are presented in Fig. 3 and we find that 37% of the BH-GS binaries have formed a stable triple system during their in-cluster evolution. These systems have an high average outer orbit eccentricity ( $e = 0.94$ ), and an average semi-major axis ratio ( $a_{\text{in}}/a_{\text{out}} = 0.004$ ).

Among the ejected population, we find that 13 BH-GS progenitors were in a stable triple system at the moment of ejection. These systems are the same triple systems with an inner BH-MS inner binary discussed in Section 3.

The BH-GS retained binaries are shown in Fig. 4. The distribution of BH masses show the same cut-off at  $45 M_{\odot}$  found in the BH-MS case (Fig. 2). The mass distribution of GSs is similar to the one found for BH-MS binaries, although we notice that the low mass part of the distribution is now mostly populated by primordial binaries. We

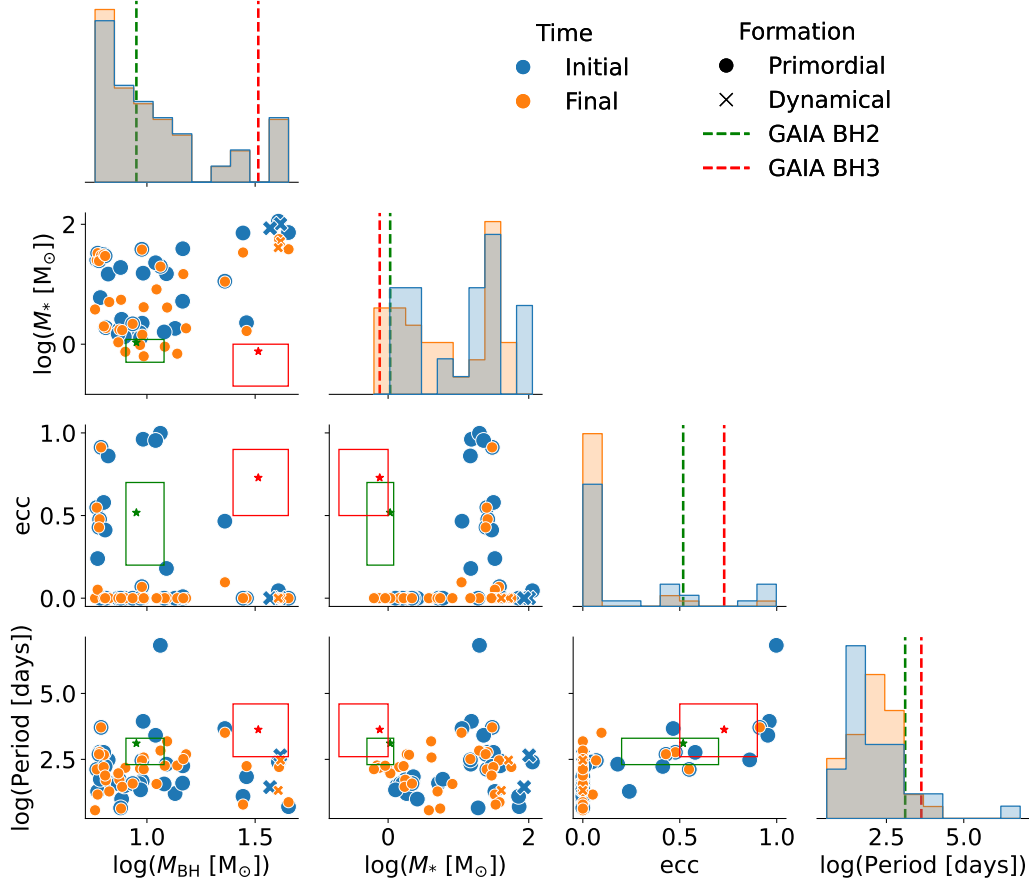


**Figure 3.** Properties of the BH-GS ejected binaries produced in our models. The dots and the crosses represent primordial binaries and dynamical binaries, respectively. The binaries at the first BH-GS time are shown in blue, the last BH-GS time is represented by orange colour. The green and red contours are the Gaia BH2 and Gaia BH3 similarity regions.

note that the three BHs that have a mass above the PPI limit in the whole sample are part of the in-cluster population. The most massive among them has a mass of  $225 M_{\odot}$ .

## 5 BH-WD BINARIES

In this section, we consider ejected BH-WD binaries. WD stars are defined following the BSE classification (indices 10, 11 and 12). The results are reported in Fig. 5.

The number of BH-WD binaries formed is given in Table 2; 22% of the ejected BH-WD binaries are formed before the ejection, the remaining are formed during the isolated evolution after ejection. Fig. 5 shows that, as expected, the properties of the binaries remain essentially the same during the lifetime of the systems. The BH mass distribution is peaked around  $M_{\text{BH}} \approx 8 M_{\odot}$ , with the exceptions being massive, dynamically formed systems. The WD masses are concentrated around  $M_{\text{WD}} \approx 1.1 M_{\odot}$ , with an extended lower mass tail. However, we note that this peak is likely strongly dependent on the max simulated time of our clusters (3 Gyr) since there are many more low mass stars which have not had time to collapse to a WD. Similarly to the BH-MS and BH-GS systems, the eccentricity has a strong peak at  $e \approx 0$ , and, as before, the reason are CE phase and tidal friction: 68% of the BH-WD progenitors experience at least one RLO event and 67% of the systems undergo a CE event before

ejection, which reduces the eccentricity from a median  $\approx 0.18$  to  $e \approx 0$ . During almost all the RLO events, the CE phase is present.

The percentage of BH-WD progenitors that undergo at least one CE is higher than for BH-MS and BH-GS. BH-WD binaries are more likely to undergo several CE and RLO phases during their evolution, therefore their eccentricity distribution is more strongly peaked at  $e \sim 0$  than BH-MS and BH-GS binaries. Although, we note that the previously mentioned caveat should be considered here since BH-WD binaries that are formed after the current max simulation time will most likely form dynamically between a lone WD and BH. These binaries will then not experience CE or RLO phases.

The CE phase and tides alone could fully explain the eccentricity and period distributions in Fig. 5. There are two exceptions: a dynamically formed system and a primordial one. The former is formed dynamically and its separation is sufficiently high to avoid CE or strong tides, the latter is formed inside the stellar cluster and it is discussed below. We find that 19% of BH-WD systems are formed dynamically.

We study the possible impact of a tertiary in the formation of the ejected population of BH-WD systems: 4 (19%) BH-WD binaries have been in a stable triple system during their in-cluster evolution, with all the inner binaries from the primordial binary population. Only 1 BH-WD system progenitor was found in a stable triple system at the moment of ejection. The semi-major axis ratio at the last time the triple existed in the cluster model is  $a_{\text{in}}/a_{\text{out}} = 0.04$ , and the eccentricity of the outer orbit is  $e = 0.95$ .

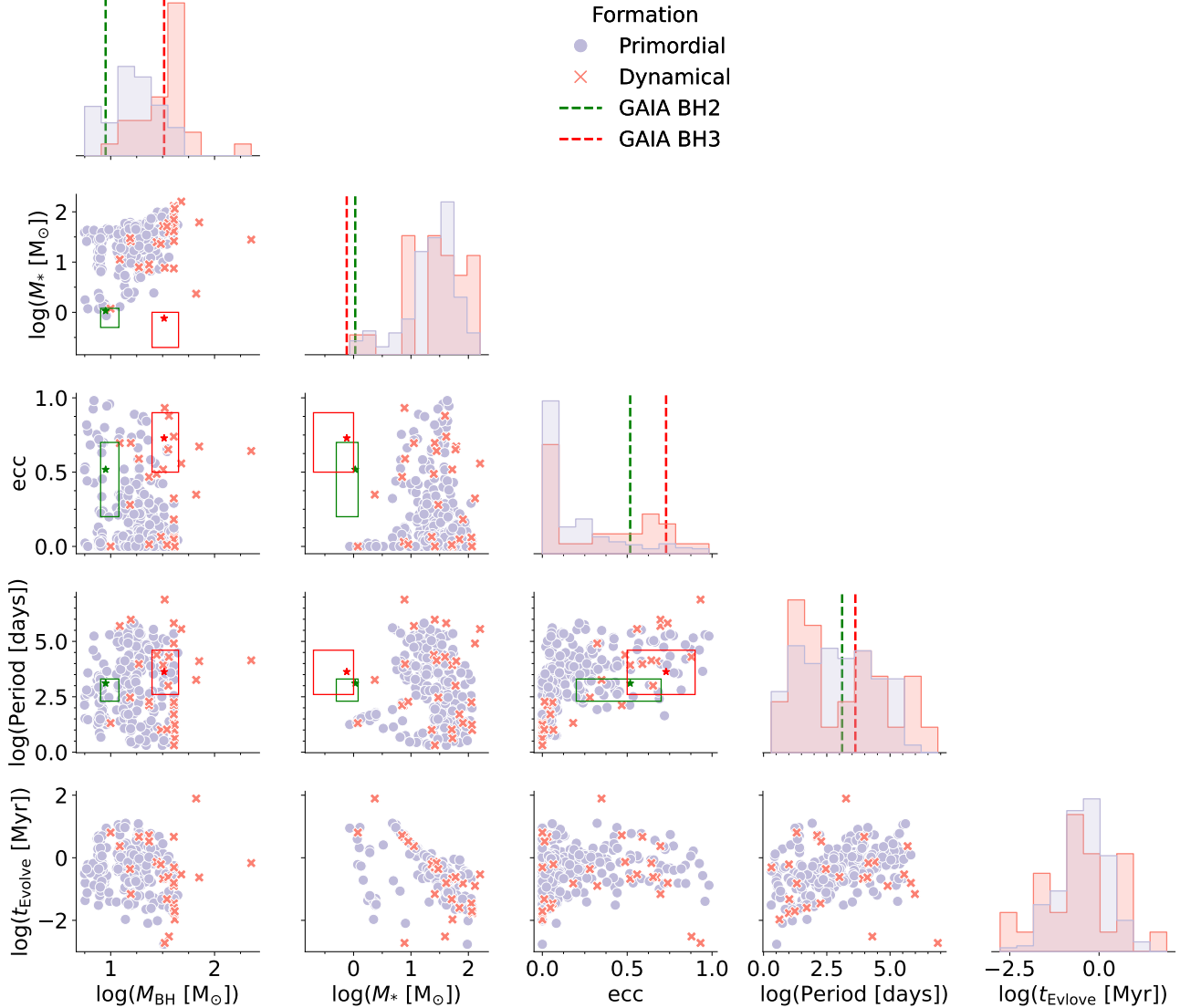


**Figure 4.** Properties of the retained BH-GS binaries. The red dots and the blue crosses represent primordial binaries and dynamical binaries respectively; the green and red contours are the Gaia BH2 and Gaia BH3 similarity region, respectively. Here  $t_{\text{evolve}}$  represents the lifetime of the binary, i.e., the time between formation and when the stellar component evolves off the giant phase.

The highly eccentric primordial binary mentioned previously has a stable triple during its in-cluster evolution: this system avoids a CE phase and the orbit becomes highly eccentric due to triple dynamics. In the other 3 stable triples, the inner binary undergoes a CE phase during which its orbit circularises and the period decreases. Because the distance of the tertiary to the inner binary is relatively large, it seems unlikely that after a CE phase the presence of the tertiary companion can significantly affect the binary evolution.

It should be stressed that the importance of the dynamical effects is strongly dependent on the characteristics of the triple system, such as the mass of the tertiary, the separation and the inclination. Moreover, the relativistic precession of the inner binary orbit can suppress the eccentricity evolution (Blaes et al. 2002), but this effect is not included in our simulations.

Finally, we looked for retained BH-WD binaries, and only found one dynamical binary with  $M_{\text{WD}} = 0.65 M_{\odot}$ ,  $M_{\text{BH}} = 67.92 M_{\odot}$ ,  $e = 0.5$  and period = 10 days. Most BH-WD binaries that are formed

in the models are immediately disrupted or ejected by dynamical encounters.

## 6 NS-S BINARIES

In this section we consider NS-S binaries, where we account for both MS and GS companions. The binary properties for the ejected population are shown in Fig. 6. We find that all but two of the ejected NS-S systems are formed before the ejection from the cluster, and that they all come from the primordial binary population. The latter point can be explained by considering that it is more difficult for a NS to capture a companion through dynamical interactions as the central region of the cluster, where these interactions typically occur, is dominated by BHs until the end of the simulation. This difficulty in forming NS-S binaries dynamically in star clusters has also been found by previous work (Tanikawa et al. 2024).

The NS masses are distributed uniformly across the interval



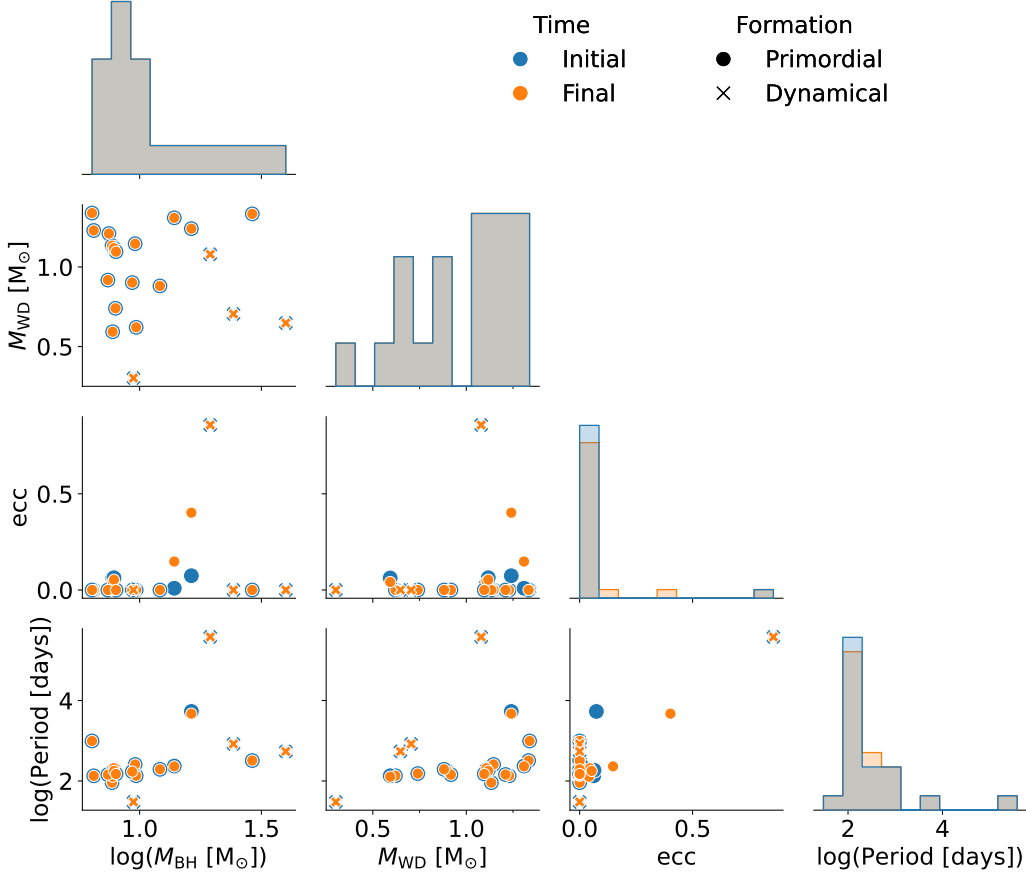


**Figure 5.** Properties of the BH-WD ejected binaries, the dots and the crosses represent primordial binaries and dynamical binaries respectively; the binaries at the first BH-WD time are shown in blue, the last BH-WD time is represented by orange colour.

$M_{\text{NS}} \in [1, 2] M_{\odot}$ , while the stellar mass distribution of the companion is peaked around  $M_* \approx 30 M_{\odot}$ , with some less massive stars down to  $M_* \approx 3 M_{\odot}$ . The eccentricity distribution is closer to uniform compared to the BH-GS or BH-WD cases (see Section 4 and Section 5). Several factors must be accounted for when considering the eccentricity distribution.

While NS-S progenitors maintain an almost circular orbit throughout their evolution, the NS natal kick increases the eccentricity of the binaries when the NS is formed. For this reason, we expect higher eccentricities than for BH-GS and BH-WD binaries. In the latter systems, CE and RLO occur shortly before the BH forms which circularises the binary, and then the reduced BH natal kick is not sufficient to produce a large spread in the eccentricity distribution. Moreover, due to the fallback prescription, a significant fraction of BHs can be formed without a natal kick.

We find that 37% of the ejected NS-S systems undergo a CE phase and that 97% experience a RLO event. In essentially all cases, the RLO and CE phases occur when the companion star is on the HG, and often the binary does not survive up to the GS phase of the companion. These behaviours explain the absence of the peak at  $e \approx 0$  in Fig. 6.

Although we find no ejected NS-S binaries in stable triple systems at the time of ejection, we do find that the 32% of the progenitor systems have been part of a stable triple system inside the cluster. We investigate these progenitor triple systems and find that they have an average semi-major axis ratio of  $a_{\text{in}}/a_{\text{out}} = 0.0001$  – the smallest through all the type of triple systems studied in this article. In fact

the average semi-major axis of the inner binary ( $\approx 100 R_{\odot}$ ) is more than five times smaller than for all the other triple systems previously mentioned ( $\approx 580 R_{\odot}$ ). Moreover, these NS-S progenitor triples have the largest average outer semi-major axis across all other triple systems, and the average outer eccentricity is  $e_{\text{out}} = 0.96$ .

We show the properties of the retained NS-S binaries in Fig. 7 and similar to the ejected population, we find only systems from the primordial binary population. The distribution of the NS masses is uniform between  $1.1 M_{\odot}$  and  $1.9 M_{\odot}$ , while the distribution of stellar masses (both MS and GS) is peaked around  $30 M_{\odot}$ . The binary eccentricities are spread between 0 and 1, with a slight preference for high eccentricities likely due to the NS natal kick. The binary periods are found predominantly between 1 day and 100 days, peaking at around  $\approx 18$  days. We only find 4 systems exceeding 100 days.

## 7 APPLICATION TO GAIA BLACK HOLES

In this section we investigate the formation of Gaia BH-like systems (El-Badry et al. 2022, 2023c; El-Badry 2024) in our simulations: We identify the top candidates within the sample, outline the formation pathways of these systems, and analyse the formation efficiencies of Gaia-like systems in our models. Similar studies can be found in Marín Pina et al. (2024), Rastello et al. (2023), Di Carlo et al. (2024) and Tanikawa et al. (2023a).

To quantify the capability of forming a certain type of systems in

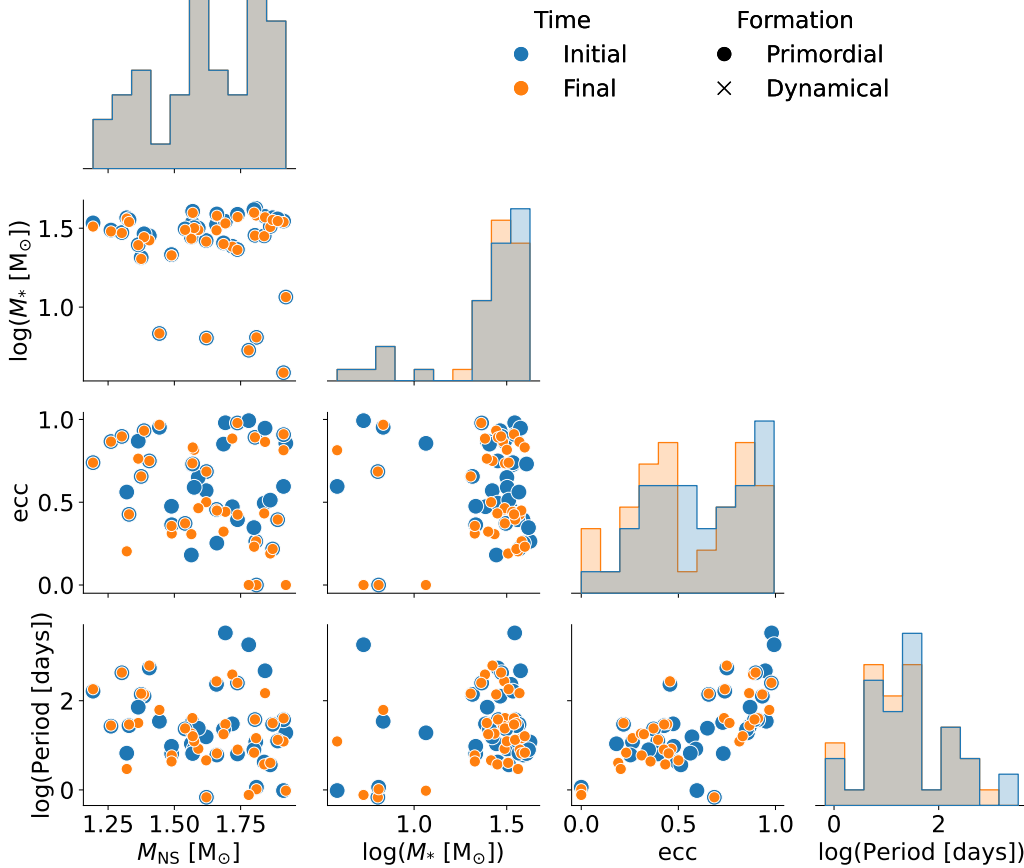


**Figure 6.** Properties of the ejected NS-S binaries. The binaries at the time the system is first classified as a NS-S are shown in blue, the last NS-S time is shown in orange. Note the absence of dynamically formed binaries.

our simulations, we define the formation efficiency as:

$$\eta = N_{\text{BH-type}}/M_{\text{tot}}, \quad (3)$$

where  $N_{\text{BH-type}}$  is the number of binaries of a certain category (BH-MS, BH-GS or Gaia-like binaries) and  $M_{\text{tot}}$  is the total mass of the cluster in our simulations or of a certain type (e.g., clusters with the same metallicity or density). Here, Gaia-like binaries mean all binaries that fall within the contour similarity regions given in Fig. 1 and Fig. 3. As shown in these figures, there is no ejected binary that satisfies all observational constraints at once. It is also evident that the constraint on the eccentricity poses a strong limit for our sample. If we relax this analysis by removing completely the eccentricity constraint, we find that there are two systems that are within the Gaia BH1 similarity region, and two systems that lie within the Gaia BH2 similarity region. However, even after relaxing the eccentricity constraint, we do not find any Gaia BH3-like system and therefore only consider Gaia BH1 and BH2 in what follows.

The relaxation of the eccentricity constraint is justified by the considerable uncertainty in the prescription for binary eccentricity evolution within the BSE framework. Finally we stress that for each system, we consider it within the similarity region if at any point during the evolutionary stage it is within the contours and not necessary at the first/last moment.

The two Gaia BH1-like ejected systems both have a dynamical formation. The first system is a dynamically formed binary from a dense ( $\rho_h = 10^5 M_\odot \text{pc}^{-3}$ ), relatively low mass ( $M_c = 10^4 M_\odot$ ) cluster, with a sub-solar metallicity ( $Z = 0.001$ ) and an initial binary

population. The second system is also formed dynamically, and it is ejected from a low density ( $\rho_h = 1200 M_\odot \text{pc}^{-3}$ ), intermediate mass ( $M_c = 10^5 M_\odot$ ) cluster, with sub-solar metallicity ( $Z = 0.001$ ) and zero initial binary fraction (i.e. no primordial binaries). The second system is also the ‘closest’ to Gaia BH1 in parameter space and it is further considered in 7.1. The efficiency for Gaia BH1-like systems considering the entire mass of the clusters ( $M_{\text{tot}} \simeq 4.6 \times 10^6 M_\odot$ ) is  $\eta = 4.36 \times 10^{-7} M_\odot^{-1}$  which is comparable to the value found by Rastello et al. (2023) in clusters with lower mass and density.

The two Gaia BH2-like systems have a primordial origin: the first system formed in a dense, intermediate mass cluster ( $\rho_h = 10^5 M_\odot \text{pc}^{-3}$ ,  $M_c = 5 \times 10^4 M_\odot$ ), with sub-solar metallicity ( $Z = 0.001$ ). This system is described in detail in section 7.2. The second system is also a primordial binary ejected from an intermediate dense cluster ( $\rho_h = 10^4 M_\odot \text{pc}^{-3}$ ), with mass  $M_c = 10^5 M_\odot$ , sub-solar metallicity ( $Z = 0.001$ ). Considering the absence of a proper eccentricity constraint for these systems, it is important to underline that both Gaia BH2-like systems undergo at least one RLO and CE phase during their evolution. In particular, the second system escapes the cluster due to a BH natal kick. Its eccentricity at ejection is  $e \simeq 0.5$ , and it is subsequently circularised during a RLO event. We find that the formation efficiency for Gaia BH2-like systems is also  $\eta = 4.36 \times 10^{-7} M_\odot^{-1}$ .

We quantify the formation efficiency of our models in producing BH-S binaries in Fig. 8. There we show the total production efficiency for all (ejected and retained) BH-S binaries and also for only ejected BH-S binaries. We then further plot the formation efficiency

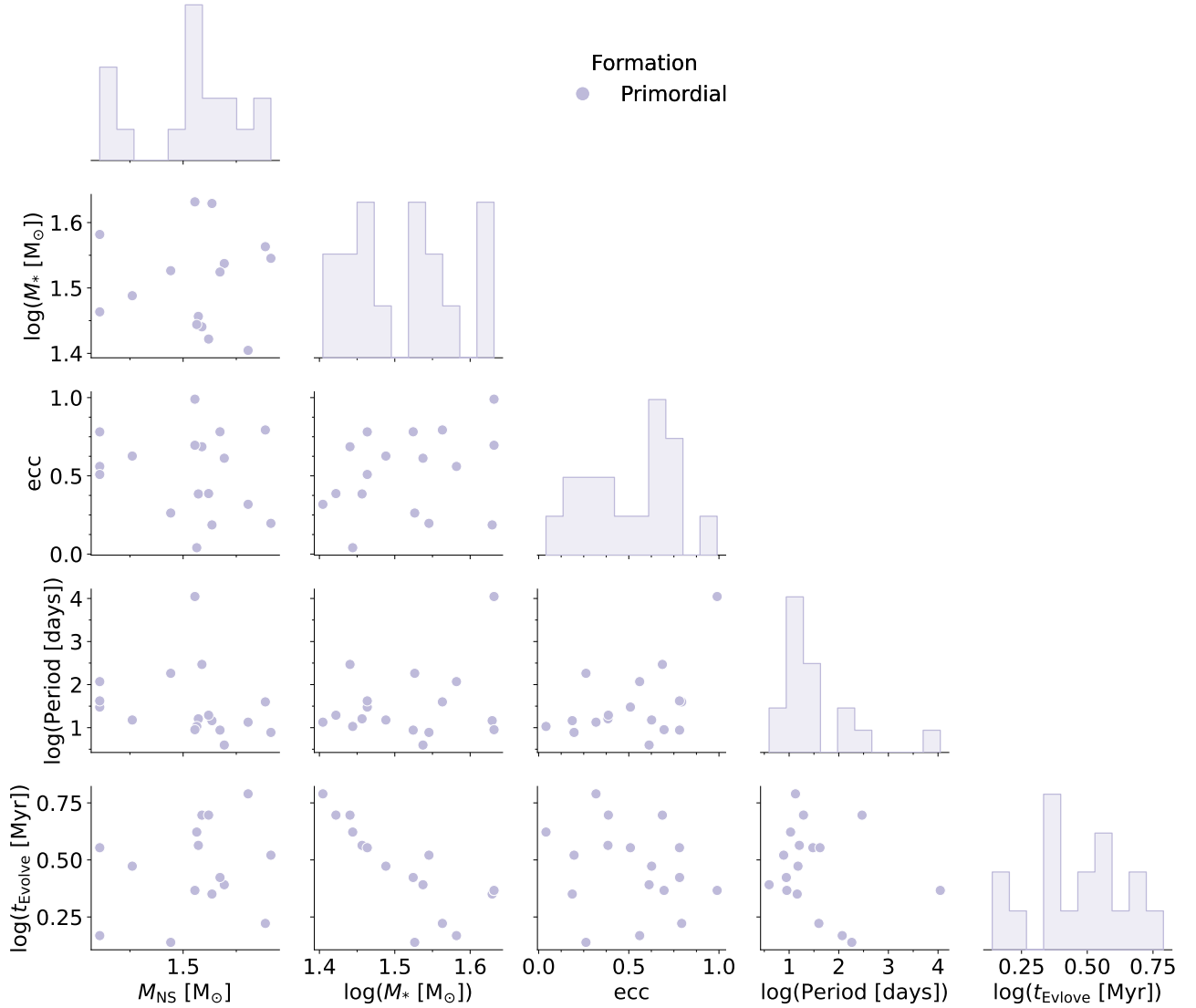


**Figure 7.** Properties of the retained NS-S binaries. We do not show the dynamically formed binaries as there are none in the sample. Here  $t_{\text{evolve}}$  represents the lifetime of the binary, i.e., the time between formation and when the stellar component evolves off the MS or giant phase.

of ejected BH-MS and BH-GS binaries separately. We plot these efficiencies both as a function of  $Z$  and  $M_c$ , and separating clusters by  $\rho_h$ . The efficiency shows a strong peak around  $Z = 10^{-3}$ , and decreases in high mass clusters for both ejected and retained binaries. There are no ejected or retained BH-S binaries in the highest mass clusters and there are two main reasons for this. First, the high mass of the cluster means a higher escape velocity, making it more difficult for binaries to be ejected in dynamical interactions. Secondly, the most massive simulations ( $M_c \geq 5 \times 10^5 M_\odot$ ) ran for a shorter time than the less massive ones ( $\leq 608$  Myr), which leads to a lower number of binaries being produced dynamically per unit mass. Furthermore, we note that the efficiency production of ejected BH-S binaries increases with cluster density, but it remains nearly independent of density for the retained population. This suggests that retained BH-S binaries mostly form from the evolution of the primordial binary population with little effect from dynamics. Our previous analysis of the retained BH-MS and BH-GS binaries (Fig. 2 and Fig. 4 respectively) supports this since we show that they are predominantly formed from the primordial binary population.

### 7.1 Best Gaia BH1 match

To identify the binary in our model that most closely resembles Gaia BH1, we follow Di Carlo et al. (2024). The distance between a point in the parameter space and a Gaia system is defined as  $|x - x_{\text{Gaia}}|/x_{\text{Gaia}}$ , where  $x$  is the array of parameters of the binary and  $x_{\text{Gaia}}$  are the parameters for Gaia BH1 reported in Table 1. Following Di Carlo et al. (2024), we do not take the eccentricity of the binary into account for distance computation, as we assume that the eccentricities remain uncertain during BSE evolution as stated earlier.

The parameters of the closest system to Gaia BH1 are reported in Table 3. The system is a dynamically formed BH-MS binary which is formed early in the cluster ( $\sim 6$  Myr) due to the encounter between a  $12.7 M_\odot$  naked He star and a low mass MS star ( $M_* \approx 0.5 M_\odot$ ). The He star rapidly ( $t \approx 0.02$  Myr) explodes in a supernova, producing a kick that expands the orbit (from  $a \approx 32 R_\odot$  to  $a \approx 175 R_\odot$ ) and makes it highly eccentric (from  $e \approx 0$  to  $e \approx 0.85$ ). The SN remnant is a stellar-mass BH with  $M_{\text{BH}} \approx 9.5 M_\odot$ . The system exists in the cluster for only  $\approx 1$  Myr before it is ejected, with velocity  $v_{\text{esc}} =$

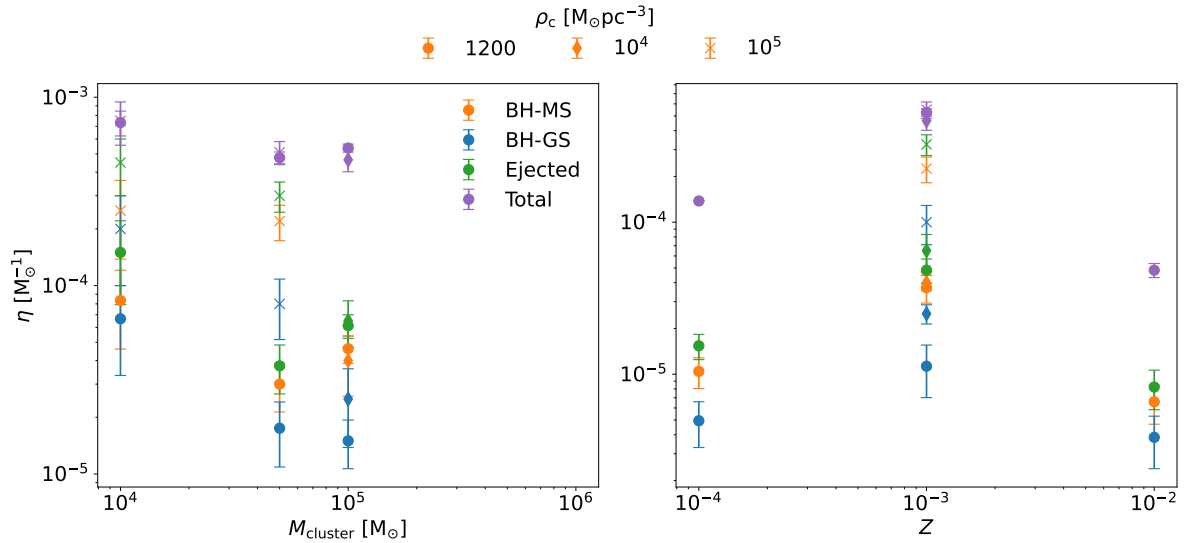


**Figure 8.** Here we show the formation efficiency of the ejected BH-S binaries split into BH-MS and BH-GS systems, as a function of initial cluster mass (left panel) and cluster metallicity (right panel). We distinguish between initial cluster half-mass density by varying marker symbols. For each cluster type we also show the formation efficiency for the ejected binary population and the total population (ejected + retained binaries).

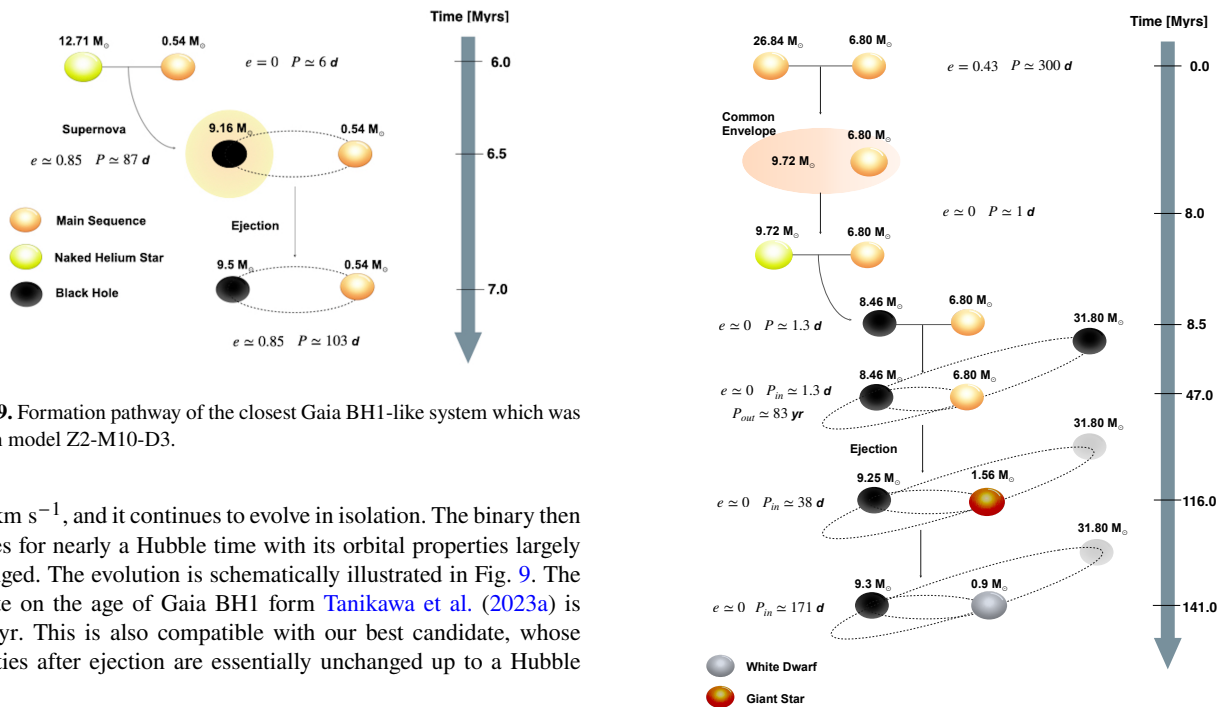


**Figure 9.** Formation pathway of the closest Gaia BH1-like system which was found in model Z2-M10-D3.

$125.3 \text{ km s}^{-1}$ , and it continues to evolve in isolation. The binary then survives for nearly a Hubble time with its orbital properties largely unchanged. The evolution is schematically illustrated in Fig. 9. The estimate on the age of Gaia BH1 from Tanikawa et al. (2023a) is  $\gtrsim 1 \text{ Gyr}$ . This is also compatible with our best candidate, whose properties after ejection are essentially unchanged up to a Hubble time.

## 7.2 Best Gaia BH2 match

In this section, we describe the closest system to Gaia BH2, with the same criteria as in Section 7.1. The parameters of the closest system to Gaia BH2 are reported in Table 3.

The system is formed as a primordial binary in a dense cluster with  $\rho_h = 10^5 \text{ M}_\odot \text{ pc}^{-3}$ ,  $M_c = 5 \times 10^4 \text{ M}_\odot$ , and  $Z = 0.001$ ; the orbit has a medium eccentricity ( $e = 0.43$ ) and a semi-major axis  $a = 607.5 \text{ R}_\odot$ ; the masses of the MS stars are  $M_1 = 26.84 \text{ M}_\odot$  and  $M_2 = 6.80 \text{ M}_\odot$ . The most massive star quickly leaves the MS, starts burning Helium in the core evolving into a naked helium star and losing 64% of its mass within 8 Myr. During this time, the evolving

**Figure 10.** Formation pathway of the nearest Gaia BH2-like system; the inclination of the orbit is represented symbolically, with the actual inclination being  $25^\circ$ . The tertiary component after ejection is shaded to emphasize that evolution continues only for the inner binary, while the tertiary is disregarded post-ejection. This system is found in model Z2-M5-D5.

star fills its Roche lobe and then enters a CE phase that circularises and shrinks significantly the orbit ( $e = 0.0$ ,  $a = 11.2 \text{ R}_\odot$ ). After 0.5 Myr, the massive star collapses and forms a BH with  $M_{\text{BH}} = 8.46 \text{ M}_\odot$ . Following another  $\approx 38.5 \text{ Myr}$ , the binary forms a stable triple with a tertiary BH ( $M_{\text{BH}} = 31.8 \text{ M}_\odot$ ). The triple system is wide ( $a_{\text{in}}/a_{\text{out}} \approx 0.001$ ) and thus the inner binary orbital properties

|                     | $M_{\text{BH}} [M_{\odot}]$ | $M_* [M_{\odot}]$ | $a [R_{\odot}]$ | $P$ [days] | $e$  | $M_c [M_{\odot}]$ | $\rho_c [M_{\odot} \text{ pc}^{-3}]$ | $Z$   |
|---------------------|-----------------------------|-------------------|-----------------|------------|------|-------------------|--------------------------------------|-------|
| Closest to Gaia BH1 | 9.16                        | 0.54              | 197.32          | 103.12     | 0.85 | $10^5$            | 1200                                 | 0.001 |
| Closest to Gaia BH2 | 9.27                        | 1.07              | 208.28          | 108.31     | 0.0  | $5 \times 10^4$   | $10^5$                               | 0.001 |
| Closest to Gaia BH3 | 9.55                        | 0.76              | 187.86          | 93.01      | 0.0  | $10^5$            | 1200                                 | 0.01  |

**Table 3.** Properties of the closest to Gaia BH systems as well as the key properties of the cluster where they are formed.

are not significantly perturbed by the tertiary. The binary is ejected from the cluster (with the tertiary still bound) as a BH-MS after 50 Myr with an escape velocity  $v_{\text{esc}} = 11.4 \text{ km s}^{-1}$ . Soon after the ejection, the MS star crosses the HG, moving into the red giant phase and slowly stripping its envelope. During this phase, the winds from the evolving star widen the orbit. Finally, 141 Myr from the start of the simulation, the star collapses into a Carbon-Oxygen WD with  $M_{\text{WD}} = 0.9 M_{\odot}$  in a circular orbit ( $e \simeq 0$ ,  $a = 281.4 R_{\odot}$ ,  $P = 171.12$  days) with a BH of  $M_{\text{BH}} = 9.3 M_{\odot}$ .

The schematic representation of this evolution is shown in Fig. 10. During the red giant phase, the properties of the system (reported at the closest moment in Table 3) are quite different than the ones measured for Gaia BH2. Moreover, the age of the system is  $\simeq 116$  Myr, which is also different from the estimated age of Gaia BH2 ( $\gtrsim 5$  Gyr).

## 8 DISCUSSION

We investigated the population of BH-star binaries formed in 32 of  $N$ -body simulations of dense and massive star clusters. Compared to previous  $N$ -body simulations which focused on low mass clusters ( $M_c \in [10^2, 10^4] M_{\odot}$ ), we have explored more massive clusters in the range  $M_c \in [10^4, 10^6] M_{\odot}$ . The formation of Gaia BH1 in low mass clusters was investigated in Rastello et al. (2023). They provide  $3.5 \times 10^4$  direct  $N$ -body simulations of clusters with an initial mass between  $3 \times 10^2 M_{\odot}$  and  $3 \times 10^4 M_{\odot}$  at solar metallicity ( $Z \simeq 0.02$ ) and define Gaia BH1 binaries with the similarity regions reported in Section 3. They find one ejected Gaia BH1 like system and compute a formation efficiency from all their models of  $\eta \simeq 2 \times 10^{-7} M_{\odot}^{-1}$ . This result is compatible with the value of  $\eta \simeq 4 \times 10^{-7} M_{\odot}^{-1}$  found in our study. However, we note that we have not considered any eccentricity constraint and both our Gaia BH1 candidates come from sub-solar metallicity clusters ( $Z = 0.001$ ).

Tanikawa et al. (2023a) studied the formation of Gaia BH1-like systems using 100  $N$ -body simulations with cluster masses  $\simeq 10^3 M_{\odot}$  and metallicity  $Z = 0.005$ . They define Gaia BH1-like binaries as those with properties such that  $M_* \leq 1.1 M_{\odot}$ ,  $P \in [100, 2000]$  days and  $e \in [0.3, 0.9]$  and they find  $\eta \simeq 10^{-5} M_{\odot}^{-1}$ . Adopting the same contours (and as before setting no constraint on eccentricity), for our BH-MS sample, we obtain a smaller  $\eta \simeq 1.52 \times 10^{-6} M_{\odot}^{-1}$ . As previously underlined in Rastello et al. (2023), the difference in the initial conditions in Tanikawa et al. (2023a) can have an impact on the number of Gaia BH-like systems and efficiencies. In particular, they set a binary fraction of 100% whilst we opt for a total initial binary fraction of 0.25%, which is 100% among BH progenitors. Both these factors could explain the larger number of Gaia BH1-like systems formed in Tanikawa et al. (2023a).

Our simulations explore masses and densities similar to the models in Marín Pina et al. (2024), who used the Monte Carlo simulations from Kremer et al. (2020). Our total efficiency for high mass clusters ( $M_c = 10^5 M_{\odot}$ ) is  $5 \times 10^{-5} M_{\odot}^{-1}$ , consistent although somewhat

smaller than the efficiency of  $\sim 10^{-4} M_{\odot}^{-1}$  found by Marín Pina et al. (2024) for similar cluster masses and densities.

Moreover, it is important to consider the impact of different initialisations of the stellar mass distribution across all of these studies. Half of our cluster models are initialised with all stars with  $M_* \geq 20 M_{\odot}$  in a binary system, whilst in Rastello et al. (2023) all stars with  $M_* \geq 5 M_{\odot}$  is in a binary. This choice causes the number of low mass binaries with no BH progenitor star to be higher in Rastello et al. (2023) compared to our simulations, possibly leading to a higher production efficiency of BH-S binaries through dynamical exchanges. In addition, Rastello et al. (2023) integrated their models for a larger number of initial cluster relaxation time, which was achievable due to their lower initial cluster masses. We note that for many of our models there still exists a significant BH population ( $> 20$ ) within the cluster. Thus, these clusters can still be considered "alive" for the purposes of forming new binaries. Continuing the simulation of these clusters would likely produce many more Gaia-like BH systems (especially in our massive clusters with  $O(10^2)$  BHs remaining in cluster), increasing our formation efficiency.

## 8.1 Conclusions

The primary objective of this study is to characterise the population of ejected binaries from the PeTar cluster simulations presented in Barber & Antonini (2024) (Section 2). We focus our analysis on the ejected populations of BH-MS, BH-GS, BH-WD and NS-S binaries. After the ejection, the binaries are evolved in isolation up to a Hubble time using the COSMIC population synthesis code. The distributions of the component masses and orbital properties for each of the binary types is presented in Figs. 1, 3, 5 and 6, where we also make the distinction between the dynamically formed and primordial binaries. In each of these plots we also show the properties at the first and last instance of that type of binary system. We also provide similar distributions for the retained binaries (Figs. 2, 4 and 7).

We present a qualitative analysis of the effects of RLO, CE evolution, tidal interactions and the presence of a stable tertiary on the eccentricity distribution of our population. We find that a large fraction of systems (always more than 20%) undergo a CE phase or a RLO event during the evolution, which lead to orbital circularisation and a peak at low eccentricities in the population distributions. The presence of a stable tertiary is found to be insufficient to significantly increase the inner binary eccentricity. On the other hand, the NS natal kick is the most efficient channel to produce eccentric binary systems with NS components.

We look for Gaia BH-like binaries in our sample (Section 7). We choose the regions of similarity for the three Gaia BH systems following previous literature (Rastello et al. 2023; Di Carlo et al. 2024; Tanikawa et al. 2023a; Marín Pina et al. 2024), and working under the assumption that the eccentricity of our systems is strongly influenced by the approximated prescription for CE and tides in BSE thus highly uncertain.

We present plausible candidates for Gaia BH1 and Gaia BH2 in our ejected sample, as well as a schematic their formation pathways



shown in Fig. 9 and Fig. 10. We find that Gaia BH1-like systems can form dynamically in a dense and massive star cluster. For Gaia BH2-like systems, we find two binaries that are consistent with the properties of Gaia BH2. These binaries are formed from the primordial binary population and are not assembled dynamically. However, we find all Gaia-like binaries are formed in low-metallicity clusters, which is in contrast with the higher metallicity ( $[Fe/H] \sim -0.2$ ) of the actual observed Gaia BH1 and Gaia BH2 systems. We do not find any binary that is consistent with the properties of Gaia BH3, however see [Marín Pina et al. \(2024\)](#).

Our simulations indicate that clusters can generate a diverse population of binaries consisting of BH and stellar components. Many of these binaries align with at least some of the properties observed in Gaia BH binaries. The fact that only a limited number of our simulated systems align with all the characteristics of the observed systems is likely due to low-number statistics, given that our models generated only 120 ejected BH-stellar binaries, along with considerable theoretical uncertainties in modelling binary stellar evolution. Nevertheless, two key findings stand out. Firstly, most of the ejected BH-stellar binaries in our models originate from the primordial binary population (88% for BH-MS and 94% BH-GS binaries), rather than being formed dynamically. Secondly, dynamically formed binaries tend to occupy extreme regions of the parameter space, with distributions extending toward higher values of orbital periods and BH masses compared to primordial binaries. Moreover, the stellar masses in dynamically formed systems include both the heaviest and the lightest stars in our sample.

Finally, we investigate the dependence of the formation efficiency  $\eta$  as a function of cluster properties (section 8) finding comparable overall results with previous work by [Rastello et al. \(2023\)](#) and [Marín Pina et al. \(2024\)](#). Furthermore, we found a strong dependence of the formation efficiency on cluster metallicity and mass: a decreasing trend in accordance with [Marín Pina et al. \(2024\)](#), but with slightly lower values of  $\eta$ .

## ACKNOWLEDGEMENTS

We thank Long Wang for useful discussions and for assisting with setting up and running the  $N$ -body simulations. Simulations in this paper utilised the high-performance  $N$ -body code PeTar (version 1047\_290) which is free available at <https://github.com/lwang-astro/PeTar>. We acknowledge the support of the Supercomputing Wales project, which is part-funded by the European Regional Development Fund (ERDF) via Welsh Government. JB is supported by the STFC grant ST/T50600X/1. FA and FD are supported by the UK's Science and Technology Facilities Council grant ST/V005618/1.

## DATA AVAILABILITY

The data used for this work will be freely shared upon reasonable request to the author.

## REFERENCES

Abbott B. P., et al., 2016, *Phys. Rev. Lett.*, 116, 061102  
 Abbott R., et al., 2021a, *The Astrophysical Journal Letters*, 913, L7  
 Abbott R., et al., 2021b, *The Astrophysical Journal Letters*, 915, L5  
 Balbinot, E. et al., 2024, *A&A*, 687, L3

Banerjee S., Belczynski K., Fryer C. L., Berczik P., Hurley J. R., Spurzem R., Wang L., 2020, *Astronomy & Astrophysics*, 639, A41  
 Barber J., Antonini F., 2024, Formation and evolution of binary black holes in  $N$ -body simulations of star clusters with up to two million stars ([arXiv:2410.03832](https://arxiv.org/abs/2410.03832)), <https://arxiv.org/abs/2410.03832>  
 Barnes J., Hut P., 1986, *Nature*, 324, 446  
 Belczynski K., et al., 2020, *ApJ*, 636, A104  
 Blaes O., Lee M. H., Socrates A., 2002, *ApJ*, 578, 775  
 Breivik K., et al., 2020, *The Astrophysical Journal*, 898, 71  
 Chakrabarti S., et al., 2023, *The Astronomical Journal*, 166, 6  
 Di Carlo U. N., Agrawal P., Rodriguez C. L., Breivik K., 2024, *The Astrophysical Journal*, 965, 22  
 Dosopoulou F., Kalogera V., 2016a, *The Astrophysical Journal*, 825, 70  
 Dosopoulou F., Kalogera V., 2016b, *The Astrophysical Journal*, 825, 71  
 Eggleton P., 2006, Evolutionary Processes in Binary and Multiple Stars  
 El-Badry K., 2024, *The Open Journal of Astrophysics*, 7  
 El-Badry K., et al., 2022, *Monthly Notices of the Royal Astronomical Society*, 518, 1057  
 El-Badry K., et al., 2023a, *Monthly Notices of the Royal Astronomical Society*, 518, 1057  
 El-Badry K., et al., 2023c, *Monthly Notices of the Royal Astronomical Society*, 521, 4323  
 El-Badry K., et al., 2023b, *Monthly Notices of the Royal Astronomical Society*, 521, 4323  
 Farr W. M., Sravan N., Cantrell A., Kreidberg L., Bailyn C. D., Mandel I., Kalogera V., 2011, *The Astrophysical Journal*, 741, 103  
 Fryer C. L., 1999, *The Astrophysical Journal*, 522, 413  
 Fryer C. L., Belczynski K., Wiktorowicz G., Dominik M., Kalogera V., Holz D. E., 2012, *The Astrophysical Journal*, 749, 91  
 Gaia Collaboration et al., 2024, *Astronomy & Astrophysics*, 686, L2  
 Gilkis A., Mazeh T., 2024, *Monthly Notices of the Royal Astronomical Society: Letters*, 535, L44  
 Harris W. E., Harris G. L., Alessi M., 2013, *The Astrophysical Journal*, 772, 82  
 Hobbs G., Lorimer D. R., Lyne A. G., Kramer M., 2005, *Monthly Notices of the Royal Astronomical Society*, 360, 974  
 Hurley J. R., Pols O. R., Tout C. A., 2000, *Monthly Notices of the Royal Astronomical Society*, 315, 543  
 Hurley J. R., Tout C. A., Pols O. R., 2002, *Monthly Notices of the Royal Astronomical Society*, 329, 897  
 Hut P., 1981, *A&A*, 99, 126  
 Iorio G., et al., 2024, The boring history of Gaia BH3 from isolated binary evolution ([arXiv:2404.17568](https://arxiv.org/abs/2404.17568)), <https://arxiv.org/abs/2404.17568>  
 Iwasawa M., Tanikawa A., Hosono N., Nitadori K., Muranushi T., Makino J., 2016, *Publications of the Astronomical Society of Japan*, 68, 54  
 Iwasawa M., Namekata D., Nitadori K., Nomura K., Wang L., Tsubouchi M., Makino J., 2020, *Publications of the Astronomical Society of Japan*, 72, 13  
 King I. R., 1966, *vaj*, 71, 64  
 Kotko I., Banerjee S., Belczynski K., 2024, *Monthly Notices of the Royal Astronomical Society*, 535, 3577  
 Kremer K., et al., 2020, *The Astrophysical Journal Supplement Series*, 247, 48  
 Kroupa P., 2001, *Monthly Notices of the Royal Astronomical Society*, 322, 231  
 Kruckow M. U., Neunteufel P. G., Di Stefano R., Gao Y., Kobayashi C., 2021, *The Astrophysical Journal*, 920, 86  
 Kruckow M. U., et al., 2024, *Astronomy & Astrophysics*, 692, A141  
 Küpper A. H., Maschberger T., Kroupa P., Baumgardt H., 2011, *Monthly Notices of the Royal Astronomical Society*, 417, 2300  
 Liu J., et al., 2019, *Nature*, 575, 618  
 Marín Pina D., Rastello S., Gieles M., Kremer K., Fitzgerald L., Rando Forastier B., 2024, *Astronomy & Astrophysics*, 688, L2  
 McClintock J. E., Remillard R. A., 2006, in Lewin W. H. G., van der Klis M., eds., Vol. 39, Compact stellar X-ray sources. pp 157–213, [doi:10.48550/arXiv.astro-ph/0306213](https://doi.org/10.48550/arXiv.astro-ph/0306213)  
 Moe M., Di Stefano R., 2017, *The Astrophysical Journal Supplement Series*, 230, 15

- Namekata D., et al., 2018, *Publications of the Astronomical Society of Japan*, 70, 70
- Oh S., Kroupa P., Pflamm-Altenburg J., 2015, *The Astrophysical Journal*, 805, 92
- Oshino S., Funato Y., Makino J., 2011, *Publications of the Astronomical Society of Japan*, 63, 881
- Peters P. C., 1964, *Physical Review*, 136, B1224
- Rastello S., Iorio G., Mapelli M., Arca-Sedda M., Carlo U. N. D., Escobar G. J., Torniamenti S., Shenar T., 2023, Dynamical formation of *Gaia* BH1 in a young star cluster ([arXiv:2306.14679](https://arxiv.org/abs/2306.14679)), <https://arxiv.org/abs/2306.14679>
- Sana H., et al., 2012, *Science*, 337, 444
- Sepinsky J. F., Willems B., Kalogera V., Rasio F. A., 2007, *ApJ*, 667, 1170
- Shikauchi M., Kumamoto J., Tanikawa A., Fujii M. S., 2020, *Publications of the Astronomical Society of Japan*, 72, 45
- Spitzer L., 1987, Dynamical evolution of globular clusters
- Stegmann J., Antonini F., Moe M., 2022, *MNRAS*, 516, 1406
- Tanikawa A., Cary S., Shikauchi M., Wang L., Fujii M. S., 2023a, *Monthly Notices of the Royal Astronomical Society*, 527, 4031
- Tanikawa A., Hattori K., Kawanaka N., Kinugawa T., Shikauchi M., Tsuna D., 2023b, *The Astrophysical Journal*, 946, 79
- Tanikawa A., Wang L., Fujii M. S., 2024, *The Open Journal of Astrophysics*
- Thompson T. A., et al., 2019, *Science*, 366, 637
- Wang L., Kroupa P., Jerabkova T., 2019, *Monthly Notices of the Royal Astronomical Society*, 484, 1843
- Wang L., Nitadori K., Makino J., 2020a, *Monthly Notices of the Royal Astronomical Society*, 493, 3398
- Wang L., Iwasawa M., Nitadori K., Makino J., 2020b, *Monthly Notices of the Royal Astronomical Society*, 497, 536
- Özel F., Psaltis D., Narayan R., McClintock J. E., 2010, *The Astrophysical Journal*, 725, 1918

This paper has been typeset from a  $\text{\TeX}/\text{\LaTeX}$  file prepared by the author.